Piezoelectrochemical Energy Harvesting from the Coupling of Mechanics and Electrochemistry in Lithium Ion Batteries

Zachary J Schiffer

4/25/16

Advisor: Craig B. Arnold

Submitted in partial fulfillment of the requirements for the degree of Bachelor of Science in Engineering

Department of Chemical and Biological Engineering

Materials Science and Engineering Certificate Program

Applications of Computing Certificate Program

Princeton University

This paper represents my own work in accordance with University regulations.

I authorize Princeton University to lend this thesis to other institutions or individuals for the purpose of scholarly research.

Zachary J Schiffer

I further authorize Princeton University to reproduce this thesis by photocopying or by other means, in total or in part, at the request of other institutions or individuals for the purpose of scholarly research.

Zachary J Schiffer

Princeton University requires the signatures of all persons using or photocopying this thesis. Please sign below, and give address and date.

Dedication

To three pillars of my Princeton life: Sarah Cen, cereal, and red pandas.

Acknowledgements

To start, I would like to thank my advisor, Prof. Craig Arnold, for all of his support and help throughout the past two years. His enthusiasm and endorsement of slightly crazy ideas has made my research experience truly enjoyable.

The Arnold lab is more than just an advisor, however, and I would be nothing without my lab peers, Jake, Minnie, and Carl, who were by my side for everything from changing pump oil to learning about a perpetual motion machine that "works on paper".

Over the past two years, my research has been full of many failures and some successes, and my family has always offered advice and support from afar. In particular, I appreciate their willingness to listen to my grumbles and my optimistic ideas as I moved from Plan A to Plan F and back again.

Throughout my time at Princeton, from introductory classes to my final thesis draft, my friends have always been nearby and supportive. These include my roommates over the years (Karthik, Jeremy, Joe, and Stephen), my original CBE study buddies (Kevin, Manali, and Maggie), and everyone in Charter, CBE or just random people with whom I interact. My thesis (and Princeton) has been a great experience because of them.

Last but not least, Sarah Cen deserves a tremendous thank you because she has helped me and been by my side during my entire Princeton education. Without Sarah, I would most certainly not be where I am today, and she is always an inspiration to me in all aspects of my life from research to breakfast to exercise.

Abstract

Current research on the mechanics of lithium ion batteries focuses on improving materials for energy storage and developing techniques to characterize materials during battery usage. However, mechanical properties of batteries have uses beyond improving energy storage, and in this work we explore low-frequency mechanical energy harvesting by using lithium ion batteries with graphite and lithium cobalt oxide (LCO) electrodes. Specifically, we show that by applying a stress to a lithium ion battery, we can increase its voltage and dissipate power over an external load, achieving conversion efficiencies of greater than 0.01% and a power output of 7.9 ± 0.3 nW. Because this process is related to the coupling of mechanics and electrochemistry in lithium ion batteries, we also investigate the relationship between mechanical strain and voltage. We empirically and theoretically demonstrate that dV/dQ is proportional to $d^2\varepsilon/dQ^2$ and suggest that strain can characterize materials for energy storage as well as energy harvesting applications.

Building on our theory of mechanical-electrochemical coupling, we show that the parameters that describe energy harvesting such as decay time and energy harvested are proportional to $d\varepsilon/dQ$. Thus, knowledge of an intercalation material's expansion can help determine that material's effectiveness for energy harvesting. We also propose that by compressing a battery during discharge, significantly more energy can be harvested than possible with compression at a fixed state of charge (0.12 ± 0.01 μW is harvested in the first dynamic harvesting test), but this energy is limited by the resistance of the compressed separator in many batteries. Last, we show that stress-voltage coupling should exist in systems such as capacitive mixing energy harvesters and that systems that do not use traditional battery materials could be extremely effective energy harvesters.

Table of Contents

List of Tables

List of Figures

1 Introduction

1.1 Lithium Ion Batteries

As our society consumes increasing amounts of energy and evidence indicates the risks of fossil fuels, clean energy has become an important focus of research. Accordingly, researchers are expending significant effort on renewable energy conversion and devices such as solar panels and wind turbines. In parallel, scientists are conducting research into energy storage techniques because without reliable storage methods, much of the energy produced by renewable energy sources would be wasted.

Batteries are the prototypical accessible storage device, and lithium ion batteries are among the most useful due to their high energy density and low rate of self-discharge.[1] Lithium ion batteries are found in devices ranging from cell phones to electric vehicles and will continue to remain important for these and other energy storage applications in the future. However, demand for better batteries requires constant innovation, and current batteries can be improved in areas such as capacity, cycle life, and safety. The desire to improve battery properties has prompted many research efforts over the past few decades, yet progress has been scattered and incremental; the chemistry of lithium ion batteries is the same as when they were first commercialized in the 1990s.[2]

In this work, we investigate batteries from a nontraditional perspective: as a tool for energy harvesting. Specifically, this work focuses on how lithium ion batteries can be used to convert mechanical work into electrical energy, a property that has not been explored in detail. Our primary goal is to characterize the energy harvesting process, and we suggest multiple procedures for harvesting energy from lithium ion batteries. In the course of this work, we also demonstrate a fundamental coupling between mechanics and

electrochemistry that improves our understanding of the underlying physics in battery materials and can potentially be leveraged to improve energy harvesting and energy storage with lithium ion batteries.

1.2 Mechanical-Electrochemical Coupling

1.2.1 Piezoelectrochemical Harvesting

Recent work on battery electrode mechanics has investigated how applied stresses can affect electrochemistry.[3] Essentially, previous research has found a linear correlation between applied stress on a battery and a corresponding increase in voltage, indicating that there is a fundamental coupling between battery mechanics and electrochemistry. In practice, one can take an off-the-shelf lithium ion battery, squeeze it, and then see an increase in the voltage (albeit small). While this has only been tested with commercial lithium ion batteries, this concept should apply not just to lithium ion batteries, but to any intercalation material.[3] Using this phenomenon, intercalation materials can be useful as stress sensors because they do not require a power source and have a flexible design shape, but they are unlikely to be widely utilized in this capacity because extremely large stresses (order MPa) are necessary to produce very small voltages (order 0.1 mV).[3]

Nevertheless, the coupling between mechanical stress and electrochemistry can be utilized in energy harvesting applications. Currently, piezoelectric materials are the most common materials for converting mechanical to electrical energy, often using high-frequency vibrations from the environment to produce electrical energy.[4,5] Piezoelectric materials, though, do not work very well for low-frequency mechanical oscillations below 1 Hz.[6,7] Battery intercalation materials, or "piezoelectrochemical" materials, take

advantage of the stress-voltage coupling in intercalation materials and harvest energy at extremely low frequencies (less than 1 mHz). Additionally, piezoelectrochemical materials have a higher energy density per unit volume than traditional piezoelectric materials.[8] To harvest energy using piezoelectrochemical materials, in our case lithium ion batteries, two anti-parallel batteries can be connected to an external load (such as a resistor), and small amounts of energy can be harvested at very low frequencies by squeezing one battery at a time (the details of this procedure are described below). This idea has been tested and proven in a simple, proof-of-concept setup using commercial lithium ion batteries.[8] Ongoing research in other groups has explored silicon electrodes to demonstrate a similar energy harvesting phenomenon. Silicon electrodes could potentially be a much more effective piezoelectrochemical harvesting material in the future, but they are not ready for commercial manufacturing and remain exclusively a research tool.[9]

1.2.2 Mechanics of Lithium Ion Batteries

Significant portions of this section are taken and modified from the author's publication on this work.[10]

Commercial lithium ion batteries are prototypical examples of piezoelectrochemical materials, and our understanding of how lithium ion batteries function as energy harvesting devices is limited by our understanding of the fundamental coupling between mechanics and electrochemistry in battery materials. To understand batteries as harvesters, we therefore need to study the fundamental mechanics and

electrochemistry in batteries. A basic battery is essentially a voltaic cell where ions move through an electrolyte solution and electrons travel around a circuit. However, the actual battery is much more complicated due to phenomena such as film formations, side reactions, and temperature effects.[11] While researchers can usually image materials in great detail, batteries are notoriously difficult to characterize because they are either sealed inside a case or, if open, must remain in an inert atmosphere. Imaging the internal reactions and materials during battery operation is impractical, and very few tools exist that can provide information about material evolution during battery usage.

Voltage is a common tool for characterizing battery materials during operation, particularly the derivative of voltage with respect to state of charge, dV/dQ. A cell's voltage is directly related to the chemistry of the materials, and many previous studies have investigated battery voltage and used it to identify phase transitions in materials, predict the effects of cell aging, and relate voltage to underlying chemical reactions.[12–16] In addition, many of these studies have resulted in the development of models to help understand battery material evolution by predicting voltage curves based on the fundamental physics in the battery. dV/dQ has proven to be an extremely useful tool and an accurate predictor of cell aging, but it is limited by physical constraints. Notably, electrode phase transitions are most easily viewed at slow charge rates, and the distinguishing features in a dV/dQ plot are nonexistent at high charge rates. Studies often cycle batteries at charge rates less than C/10 to glean information from dV/dQ curves.

Recent battery research has focused on mechanical properties, such as strain, ε, as an indicator of underlying phenomena.[15,17–22] This previous research relies on the fact that during battery operation, electrode materials are known to expand and contract in

repeatable patterns. Strain has been correlated with important battery properties such as state of charge and state of health, and mechanical measurements can be used to identify capacity fade, lithium plating, and more. Batteries also produce repeatable plots of stress and strain versus state of charge during cycling, analogous to plots of voltage versus state of charge.

Despite a surge in recent research on mechanical properties of batteries, battery strain remains underutilized as a tool to better understand electrode materials. A few studies have postulated that dε/dQ bears a similarity to dV/dQ and might indicate phase transitions in electrode materials.[3,17,22] However, previous work does not fully explore how or why the derivatives of strain relate to dV/dQ or what advantages strain differentials have compared to voltage. In this work, we investigate the coupling between strain and voltage with the goal of characterizing and optimizing materials for energy harvesting systems.

2 Energy Harvesting with Lithium Ion Batteries

2.1 Experimental Methods

As mentioned previously, an applied stress to lithium ion batteries will produce a change in voltage. However, this change in voltage is typically on the order of 0.1 mV and is very difficult to measure with standard equipment.[3] Our primary energy harvesting setup consists of 170 mAh pouch cells containing LCO and graphite electrodes. State of charge measurements are based on the 170 mAh nominal capacity, and batteries are charged to a given state of charge after discharging to 3 V and holding at 3 V until the current decays under 1 mA. These cells are manufactured by AA Portable Power Corp

and have a nominal size of 25 by 20 by 5 mm. They are compressed using either an Instron 5969 or an Instron 5567 and voltage measurements are taken with a Solartron 1287. All strain measurements in the Instrons use an LVDT strain gauge.

For the characterization harvesting experiments (**Section 4.1**), we connect two batteries in anti-parallel with a resistor between two leads and measure the potential drop across the resistor. A schematic of the setup is depicted in **Figure 1** and described in further detail in previous work.[8] One cell is compressed to 0.1 and 15 MPa in a cyclic pattern depicted below in **Figure 2a**. Note that each cell is cycled five times before any measurements are taken to avoid first-time inelastic effects. Additionally, measurements are only taken after the initial voltage equilibrates to circa 0 V (< 50 μV). During analysis, the voltage decay is fit with exponential functions using MATLAB and all mathematical analysis is performed in MATLAB and Excel. All error is 1σ unless otherwise indicated. For single-cell harvesting experiments (**Section 4.2**), the same testing equipment is used, but a 500 mAh lithium ion battery is used instead of a 170 mAh battery (further described in **Appendix A**).

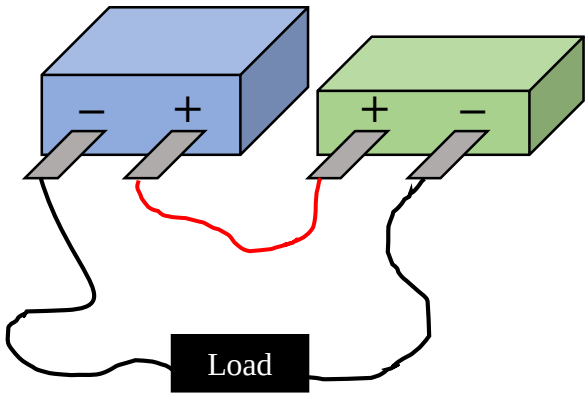

Figure 1. Schematic of experimental setup. The green cell is compressed and the blue cell is the reference cell/reservoir.[8]

2.2 Proof of Concept

As mentioned in **Section 1.2.1**, lithium ion batteries exhibit a mechanical-electrochemical coupling such that when a stress is applied, the voltage increases. Specifically, previous research has determined the following relationship.

$$\Delta V = \frac{\partial \epsilon}{\partial q_V}\sigma = k\sigma \quad [1]$$

Where ε is the strain, q_V is the volumetric charge, and k is the coupling factor.[3,8] In the setup shown in **Figure 1**, the green cell is compressed, increasing its voltage relative to the blue reference cell. However, because the two cells are connected, the voltage will equilibrate, and power will be consumed by the load. In this particular case, the load is a 10 Ω resistor (chosen to maximize power output through impedance matching).[8] Once the voltages have equilibrated, the stress is removed and the voltage of the green cell decreases relative to the blue cell. The cells then equilibrate again, generating power across the load. An example of multiple cycles is shown in **Figure 2**. The cells in this figure are at 20% state of charge. In **Figure 2a**, the stress applied as a function of time is shown, and the resulting voltage increases are shown in **Figure 2c**. In **Figure 2b**, the work done by the Instron over time is plotted. In **Figure 2d**, the energy harvested from each cycle is given as a function of time (this quantity is simply the integral of the power over the resistor with respect to time). One cycle is marked with vertical dashed lines in **Figure 2d**. In **Figure 2c**, the magnitude of the peak voltages differ during the "compressed" step and the "uncompressed" step. This is likely due to changing internal resistance during compression or the system not being fully equilibrated.[23]

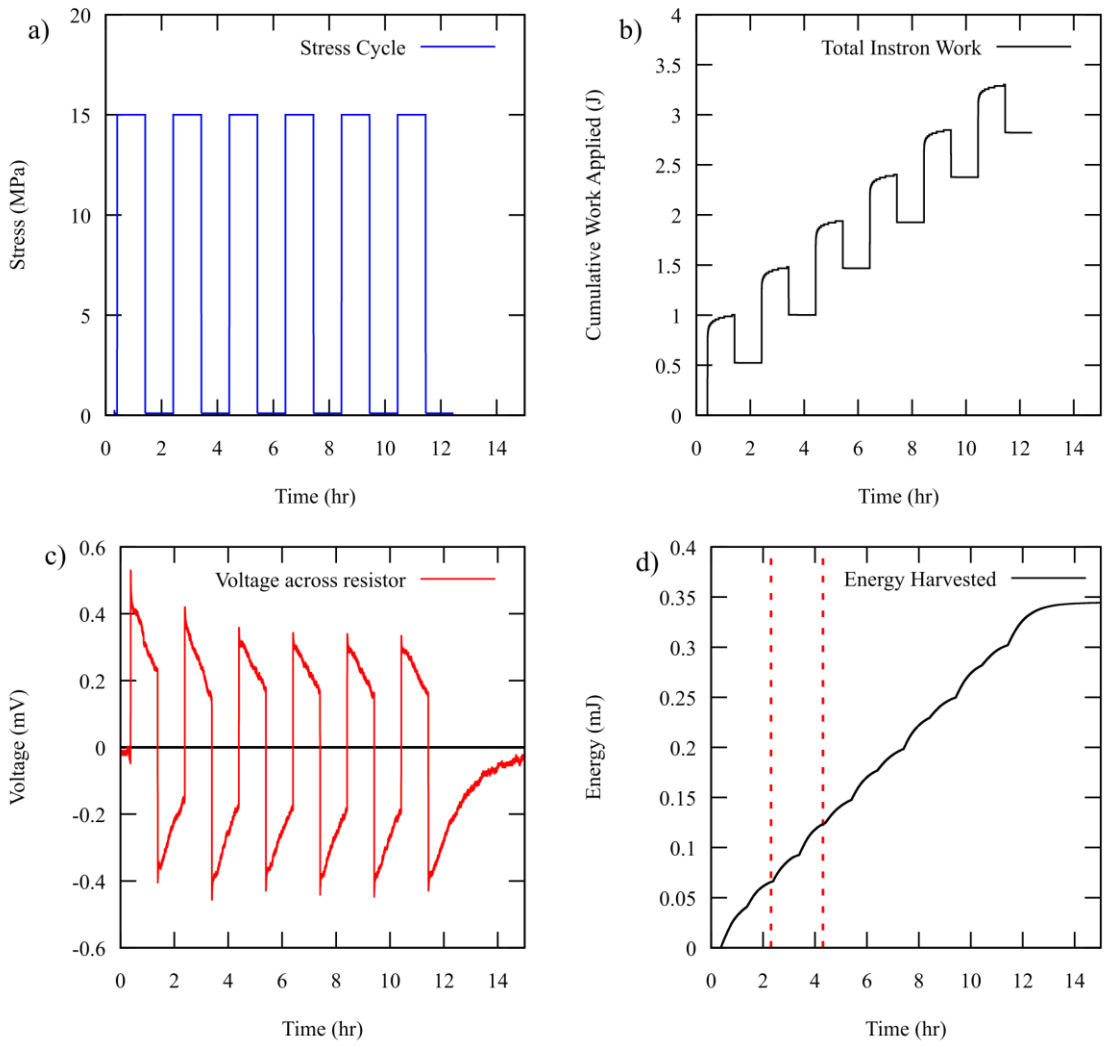

Figure 2. Demonstration of the feasibility of energy harvesting using 170 mAh batteries at 20% state of charge. The stress profile (a) and Instron work (b) are compared to the change in voltage of the harvester (c) and the energy harvested (d). The dashed lines in (d) mark a single cycle.

On average, each cycle during the test shown in **Figure 2** results in 0.057 ± 0.002 mJ of energy (average 7.9 ± 0.3 nW output) and the Instron applies 0.47 ± 0.01 J per cycle, resulting in a conversion efficiency of 0.012 ± 0.004%. Note that this is not an idealized system, and similar batteries should have efficiencies between 0.01% and 0.2% for this type of energy harvesting.[8] The large variations in expected efficiencies are because the Instron does roughly the same amount of work compressing the battery

electrodes regardless of system parameters, but the amount of harvested energy is a strong function of parameters such as state of charge. However, this efficiency is comparable to other mechanical harvesters that use mechanical-electrochemical coupling. Recent research using silicon electrodes, which in theory have a larger coupling factor (Equation 1) and should produce more energy, have found efficiencies of 0.62%, a larger but still comparable number.[9]

In **Figure 2c**, the voltage does not completely decay to 0 V during each cycle because the cycles are limited to a two hour period in order to perform more tests. Two hours is sufficient to fit an exponential, and by comparing the experimental energy harvested per cycle to the theoretical energy harvested by letting the exponential decay to infinite time, each cycle achieves 80 ± 2% of its maximum possible harvested energy if the voltage decayed infinitely. In the end, this experiment demonstrates the feasibility of energy harvesting using this procedure and provides a baseline for future piezoelectrochemical experiments and characterizations. However, to improve and optimize this procedure, we need to understand the underlying mechanical-electrochemical coupling in battery materials better. Specifically, we need to understand how the electrochemistry of the battery electrodes affects the mechanics and vice versus.

3 Strain-Voltage Coupling in Lithium Ion Electrodes

3.1 Motivation

Although **Section 2** demonstrates the feasibility of lithium ion battery energy harvesters, it does not describe the fundamental processes that make energy harvesting possible. Equation 1 relates the increase in voltage from a given stress to the derivative of strain

with respect to state of charge (dε/dQ). Most likely, the time decay of the voltage is related to this quantity and possibly other quantities such as dV/dQ. Therefore, to understand the underlying causes and processes in energy harvesting, we need to investigate the coupling between strain and voltage for lithium ion battery systems and relate them at a fundamental level.

3.2 Experimental Methods

The experimental methods from this section were implemented during the summer and are described in **Appendix A**. In **Sections 3.3** to **3.6**, portions of the data and analysis are taken from summer work by the author and are included for continuity because the research spanned the months of July to October, 2015. Additionally, much of **Section 3** is modified from the author's publication on this work in December, 2015.[10]

3.3 Comparison of Strain and Voltage Derivatives

To characterize the coupling between voltage and electrochemistry, we investigate the strain of the battery during charging. Although stress may seem the more natural mechanical property to study since energy harvesting is a function of stress, we study strain because it is more closely linked to underlying physics and electrochemistry (intercalation in materials produces strain which in turn produces stress). Strain and stress are easily related through Young's modulus. In **Figure 3**, the strain from a single charge cycle (**Figure 3a**) is displayed to aid understanding of the expansion process. Due to previous interest in dV/dQ as a tool for characterizing battery materials, we initially compare dε/dQ directly to dV/dQ (**Figure 1b**) for a battery charged at C/20. Previous

work noted that dε/dQ and dV/dQ display features at similar states of charge, yet no studies have rigorously compared strain and voltage.[3,17] Upon visual inspection, **Figure 3b** (containing dε/dQ) shows that the peaks in the dV/dQ curve align nicely with inflection points of dε/dQ (i.e., at the points between plateaus in the dε/dQ data). To quantify these points, the second derivative, $d^2\varepsilon/dQ^2$, is displayed in **Figure 3c**, revealing that each peak in the dV/dQ curve has a corresponding peak in $d^2\varepsilon/dQ^2$.

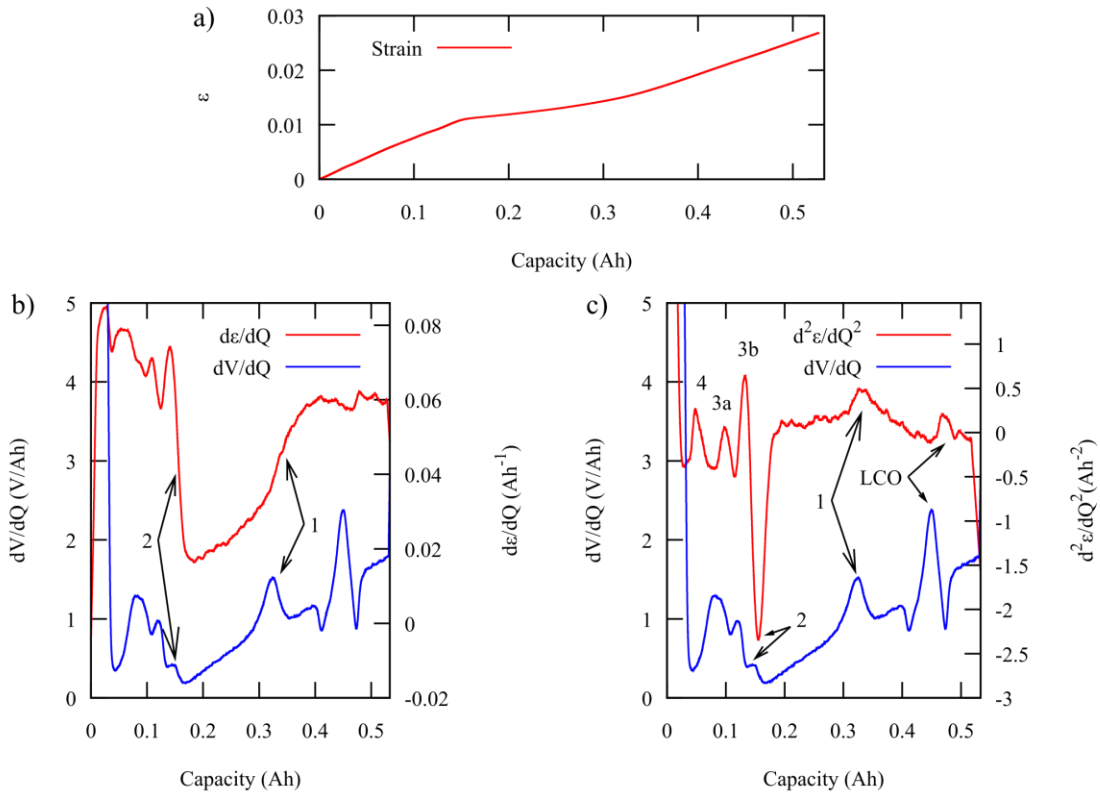

Figure 3. Strain (ε) from a single charge cycle (a), direct comparison of dε/dQ and dV/dQ (b), and $d^2\varepsilon/dQ^2$ and dV/dQ (c) for a commercial battery cycling at C/20. Select transitions are labeled and the similarity between the $d^2\varepsilon/dQ^2$ and dV/dQ peaks is visually apparent.

Because the peaks in dV/dQ correspond to electrode stage transitions, we attribute the analogous peaks in $d^2\varepsilon/dQ^2$ to electrode stage transitions. Specifically, previous

studies have shown that most of the peaks present in dV/dQ are due to the graphite electrode, and we hypothesize that the analogous peaks in $d^2\varepsilon/dQ^2$ also represent graphite transitions because the graphite electrode has more stages and exhibits an order of magnitude larger expansion than LCO.[24–26] The last peak in both the strain and voltage curves at around 0.46 Ah is a known exception and belongs to an LCO electrode transition.[15]

While peaks in **Figure 3c** are visually clear, there are multiple options for quantifying them. A quantitative comparison of dV/dQ peaks and $d^2\varepsilon/dQ^2$ peaks is given in **Appendix B**. The most important peaks used in this paper and in most analyses of batteries are the last two graphite transitions (1 and 2 in **Table B1** and **Figure 3**). These transitions have the most severe effect on the rate of expansion due to the differences in the graphite-lithium intercalation lattice height for relevant graphite phases.[27,28] The rest of the peaks in the voltage and strain data are important only because they are visible with both voltage and strain. Notably, there is no clearly defined peak for the transition from stage 3 to stage 2 in the voltage data (transition 2). Often, all of the smaller peaks in this region are lumped together as one peak or the trailing edge of this conglomerate of peaks is used to represent this transition since most analyses of graphite phases in batteries only focus on the large regions defined by transitions 2 and 1 and do not worry about the nuances in transitions before 2.[13,14]

With C/20 charging, we demonstrate the clear analogy between strain (specifically $d^2\varepsilon/dQ^2$) and voltage (dV/dQ). Moreover, the peaks present in **Figure 3c** for $d^2\varepsilon/dQ^2$ are arguably better defined than the peaks in the dV/dQ curves. In **Section 3.6**, we justify this relationship between strain and voltage with a brief theoretical rationale

based on fundamental chemistry. However, the empirical data displayed in **Figure 3** suggests that a relationship between mechanics and electrochemistry exists that can be utilized to identify and optimize energy harvesting materials.

3.4 Advantages of Strain Compared to Voltage

While the primary goal of this work is to investigate lithium ion batteries for energy harvesting applications, we also aim to improve understanding of battery materials, specifically the coupling between mechanics and electrochemistry. In particular, we propose that because strain and voltage contain the same information, strain data can potentially be used to characterize batteries for situations in which voltage data is unreliable, such as at high C-rates.

Traditionally, to produce reliable voltage derivatives and analyze electrode staging, batteries must be cycled at slow C-rates. Most reported uses of dV/dQ use rates of C/10 or below.[12–16] These rates are impractical and unrealistic for real world applications. In **Figure 4**, $d\varepsilon/dQ$, $d^2\varepsilon/dQ^2$ and dV/dQ are displayed at varying charge rates from C/20 to C/2. We demonstrate that strain can be used to determine transitions at higher charge rates than possible with voltage. In particular, transition 1 (as indicated in **Figure 3**) is extremely difficult to clearly determine with dV/dQ but is quantifiable with strain. Although we focus on the effectiveness of strain up to C/2 in this work, strain can produce reliable data at rates higher than C/2, discussed further below.

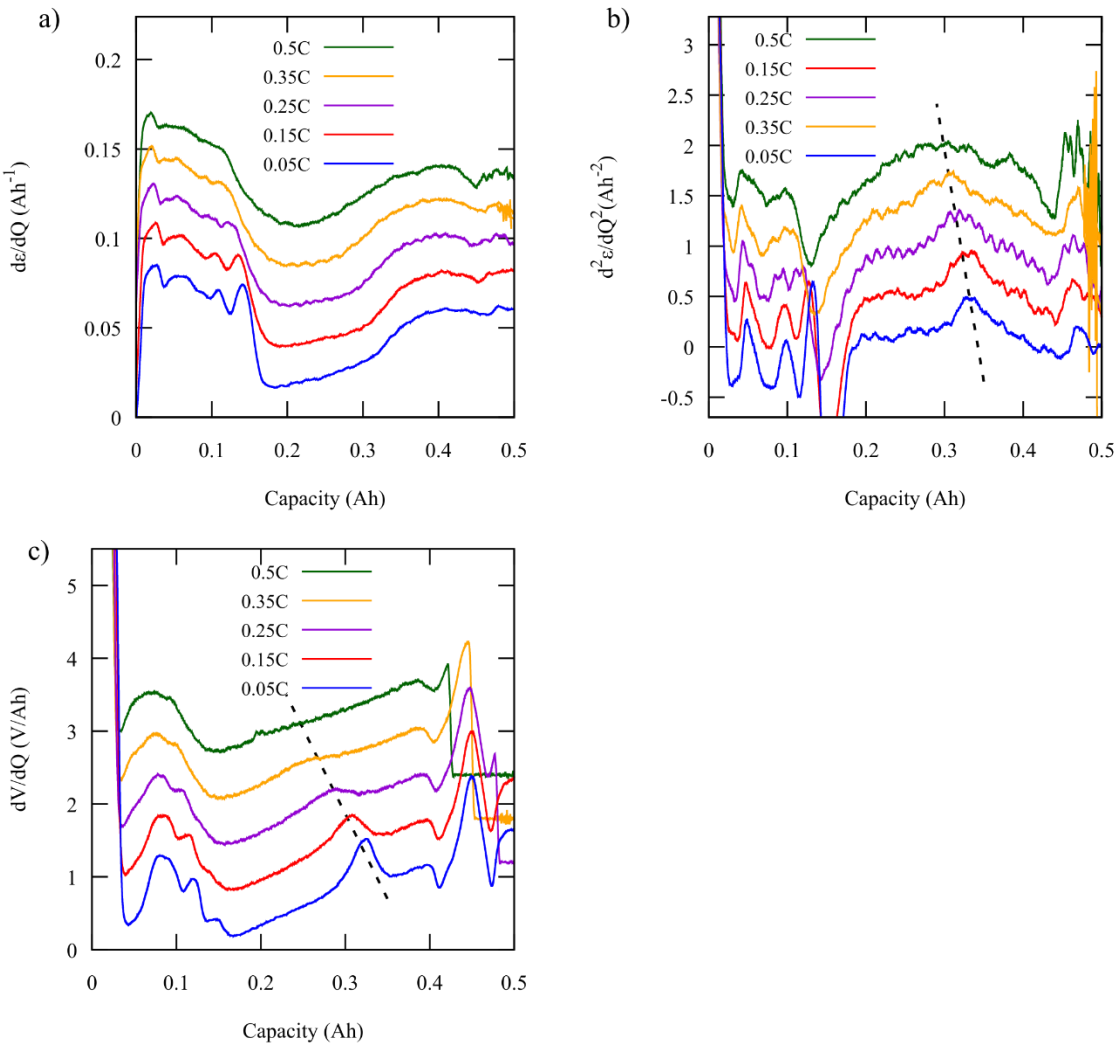

Figure 4. Comparison of dε/dQ (a), $d^2\varepsilon/dQ^2$ (b), and dV/dQ (c) at charge rates up to C/2. Dashed lines in (b) and (c) indicate transition movement as charge rate changes. Note the vanishing peak as charge rate increases in the voltage data (c) while a distinct curvature remains present in the strain data (b).

In **Figure 4a**, transitions 1 and 2 are distinct steps in the dε/dQ curve at C/20, but the transitions become slopes as the C-rate increases, giving the curve a bowl like shape. In **Figure 4b**, there is a distinct peak in the $d^2\varepsilon/dQ^2$ data at C/20 for transition 1. As charge rate decreases, this peak smooths out to a wide Gaussian, mirroring the increased curvature found in **Figure 4a**. Despite a wider and shorter Gaussian, the Gaussian is always discernable. In **Figure 4c**, transition 1 is clearly visible at C/20, but by C/4 it is

difficult to quantify, and the peak is nonexistent at C/2. This is likely due to the relatively small difference in voltage before and after the transition. When the transition occurs rapidly, dV/dQ has a smaller magnitude and is spread out over a longer period of time, making a transition peak difficult to pinpoint. The peaks in the dV/dQ curve for the transitions at lower states of charge than transition 2 merge with transition 2 into one peak at higher rates. In the strain data (**Figure 4b**), the peak for transition 2 remains distinct at C/2, and the lower transitions combine from three distinct peaks at C/20 into two peaks at C/2. Referencing **Table B1**, the peaks for transition 3a and 3b are the ones that combine.

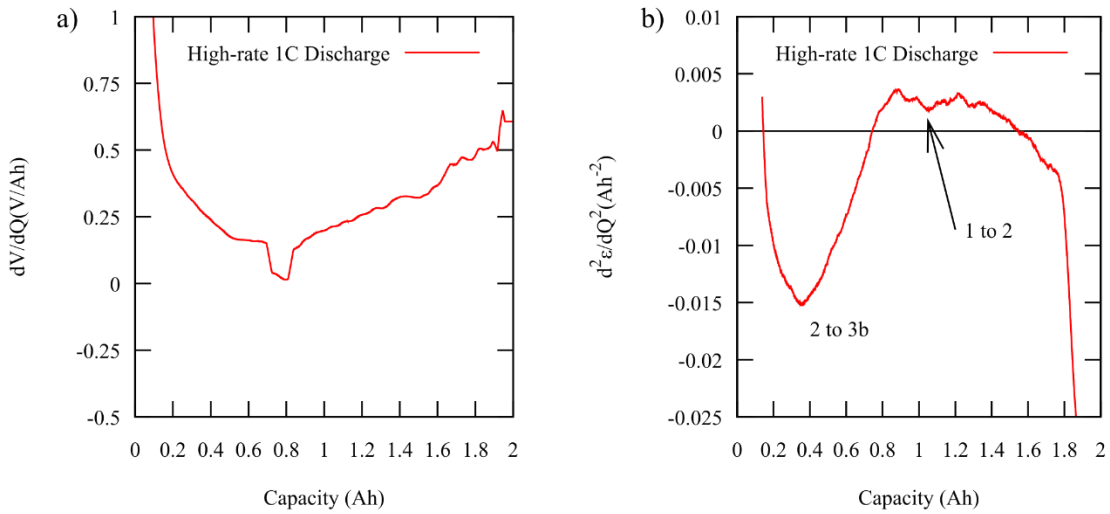

Figure 5. Comparison of dV/dQ (a) and $d^2\varepsilon/dQ^2$ (b) in the practical scenario of discharging at 1C. There are no visible peaks in the voltage data but there are definite peaks at the major transitions in the strain data. The black line in the (b) marks the 0 point, and the transitions are labeled in (b).

Using our setup, we show the transitions in the strain plots at charge rates up to C/2. However, a more realistic scenario would involve higher charge rates. We therefore use a battery designed to be discharged at rates of up to 1C to demonstrate the

applicability of strain to higher rates. In **Figure 5**, dV/dQ and $d^2\varepsilon/dQ^2$ are displayed at a discharge of 1C. The high-rate cell is necessary at 1C because batteries that are not built to charge at higher rates will exhibit lithium plating and other phenomena at 1C that would interfere with our expansion measurements. **Figure 5a** shows the lack of peaks in the dV/dQ curve at 1C, and **Figure 5b** demonstrates how the strain transitions are apparent during discharge and in a practical scenario, although an in-depth study of higher charge rates and discharge curves is beyond the scope of this paper. Specifically, the peaks for the transition from stage 1 to 2 and from stage 2 to 3b are visible in **Figure 5b** (the equivalent charge transitions 1 and 2, respectively, from **Figure 3**). Overall, the transitions are still clear in the strain data in the practical situation of discharging at 1C and possibly at even higher rates while the transitions are undetectable in the voltage data. A detailed analysis of the strain and voltage peaks as functions of charging rate is presented in **Appendix C**, yet **Figure 4** succinctly shows the benefits of understanding the coupling of strain and voltage for improved characterization of battery materials in applications other than energy harvesting.

3.5 Strain as a Tool to Predict Aging

One of the primary uses for dV/dQ is to monitor and study cell aging. Essentially, the distance between peaks in a dV/dQ curve represents how much lithium is transferred during a given stage. As the cell ages, these peaks shift according to how much lithium is lost and how the lithium is lost (i.e. lithium lost to SEI formation results in different peak shifts than those from active material in electrodes being lost). Because strain curves clearly show stage boundaries, similar trends in the strain peaks as those found in voltage

curves should be visible. An in-depth study of peak shifts and aging is beyond the scope of this work, but a quick study to determine the feasibility of using peak shifts as a tool for aging is possible. Cycling continuously at C/2 (possible with strain, but not with voltage), a single battery is cycled 50 times. In **Figure 6**, $d^2\varepsilon/dQ^2$ is displayed for the first and fiftieth cycles. Cycle number 50 is offset vertically for visibility, and transitions 1 and 2 in the graphite as well as the LCO transition are marked. For cycle one, these transitions occur at 0.306 ± 0.006 Ah, 0.131 ± 0.006 Ah, and 0.463 ± 0.003 Ah, respectively (error represents confidence based on fit and neighboring cycles). For cycle 50, these transitions occur at 0.290 ± 0.002 Ah, 0.119 ± 0.004 Ah, and 0.452 ± 0.004 Ah, respectively. The first transition shifts left by 0.016 ± 0.006 Ah, the second transition shifts left by 0.012 ± 0.07 Ah, and the LCO transition shifts left by 0.011 ± 0.005 Ah. All the transitions shift by the same order of magnitude and are within error of each other. Additionally, during this 50 cycle test, the battery lost 1.1% of its initial capacity. The shift left in all of the peaks is consistent with previous work, but a separate, longer study is necessary to conclusively propose a mechanism for capacity fade based on expansion peak shifts.[14,15]

This short aging study is a first step toward a full study investigating how strain data can quantify aging behavior instead of voltage data. Moreover, this short study solidifies the empirical relationship between strain and voltage, demonstrating that both strain and voltage indicate the electrode phase transitions and are intrinsically coupled.

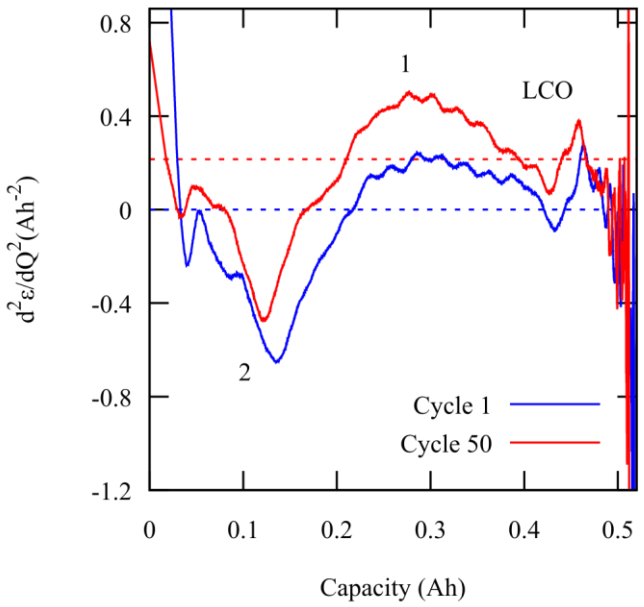

Figure 6. Comparison of $d^2\varepsilon/dQ^2$ between cycle number 1 and cycle 50. Cycle 50 cis offset vertically about 0.2 Ah^{-2} (zero point marked by dashed horizontal line), and the major transitions are labeled. The large noise at very high states of charge is due to imprecision in the numerical second derivative at the edge. The shift in the peaks due to aging is visible, similar to shifts expect in the voltage data.

3.6 Theoretical Analysis of Strain and Voltage

We have empirically shown that at slow rates, $d^2\varepsilon/dQ^2$ contains analogous peaks as those in dV/dQ that correspond to electrode staging. Yet to best use this empirical observation to develop and optimize energy harvesting materials, we need a model that theoretically relates strain and voltage.

The lithiation and delithiation of electrodes can be modeled with a chemical equation. The delithiation of LCO is a prototypical example of a cathode delithiation.

$$\nu\ Li_yCoO_2 \rightarrow \nu\ Li_{y-\frac{1}{\nu}}CoO_2 + Li \qquad [2]$$

For this reaction, the free energy of reaction is given in terms of the energy of formation for the product and reactants:

$$\Delta G_{rxn} = \nu\Delta G^f_{Li_yCoO_2}\left(y - \frac{1}{\nu}\right) + \Delta G^f_{Li} - \nu\Delta G^f_{Li_yCoO_2}(y) \qquad [3]$$

Using Li metal as a reference state, $\Delta G^f_{Li} = 0$, the above equation simplifies to:

$$\Delta G_{rxn} = \frac{\Delta G^{f}_{Li_yCoO_2}\left(y - \frac{1}{\nu}\right) - \Delta G^{f}_{Li_yCoO_2}(y)}{\frac{1}{\nu}} \quad [4]$$

If Δn moles of Li leave the LCO, where $\Delta n = \frac{1}{\nu} > 0$, then the instantaneous free energy of reaction is described by:

$$\Delta G^{LCO}_{rxn} = \lim_{\Delta n \to 0} \Delta G_{rxn} = \lim_{\frac{1}{\nu} \to \infty} \Delta G_{rxn} = -\frac{d}{dy}\left[\Delta G^{f}_{Li_yCoO_2}\right] \quad [5]$$

An analogous derivation for graphite as a model anode, using the following reaction to represent lithiation yields an expression for the free energy of reaction for graphite lithiation.

$$Li + \eta\ Li_xC_6 \rightarrow \eta\ Li_{x+\frac{1}{\eta}}C_6 \quad [6a]$$

$$\Delta G^{graphite}_{rxn} = \lim_{\Delta n \to 0} \Delta G_{rxn} = \lim_{\frac{1}{\eta} \to \infty} \Delta G_{rxn} = \frac{d}{dx}\left[\Delta G^{f}_{Li_xC_6}\right] \quad [6b]$$

The full reaction is simply the sum of the two half-reactions,

$$\Delta G^{full}_{rxn} = \frac{d}{dx}\left[\Delta G^{f}_{Li_xC_6}\right] - \frac{d}{dy}\left[\Delta G^{f}_{Li_yCoO_2}\right] \quad [7]$$

Equation 7 matches previous derivations from the literature.[28,29] While this full cell equation is very general, in the case of a phase transition in the electrode material, the equation can be simplified. Because graphite is known to have multiple phase transitions (many of the stages referred to previously are in fact phase coexistence), it is used as an example. In the graphite electrode, a transition is made from phase *i*, occurring at $x = x_i$ to phase *j*, occurring at $x = x_j$. The lithiation of graphite now represents a phase transition from $x = x_i$ to $x + \frac{1}{\eta} = x_j$. The free energy of reaction then becomes a constant

(derived by plugging in the previous bounds into a graphite equation analogous to Equation 4).

$$\Delta G_{rxn} = \frac{d}{dx}\left[\Delta G^{f}_{Li_xC_6}\right] = \frac{\Delta G^{f}_{Li_{x_j}C_6} - \Delta G^{f}_{Li_{x_i}C_6}}{x_j - x_i} \quad [8]$$

The free energy of formations for phase *i* and phase *j* are materials properties. Because each lithium atom contains a single charge, the cell voltage can be written as:

$$E_{cell} = -\frac{1}{F}\Delta G_{rxn} = -\frac{1}{F}\left\{\frac{d}{dx}\left[\Delta G^{f}_{Li_xC_6}\right] - \frac{d}{dy}\left[\Delta G^{f}_{Li_yCoO_2}\right]\right\} \quad [9]$$

Should either electrode material be in a phase transition, the respective derivative can be replaced with the constant described in Equation 8 (and an analogous equation for LCO not shown).

Here we focus on the derivatives of material strain with respect to the extent of lithiation of graphite, *x*. Like the free energy of formation, materials also have lattice constants associated with different phases. Letting c_i represent the lattice height of the i^{th} phase (where c_0 is the initial lattice height corresponding to either fully lithiated or delithiated materials), the strain in a material in a single phase is given by:

$$\epsilon_i = \frac{c_i - c_0}{c_0} \quad [10a]$$

$$\frac{d\epsilon_i}{dx} = 0 \quad [10b]$$

Should the material be in a phase transition between phases *i* and *j*, assuming a first order phase transition and short diffusion lengths for lithium, the strain of the material will increase at a constant rate determined by the known lattice heights of the two bounding phases.

$$\epsilon_{i,j} = \frac{c_{i,j} - c_0}{c_0} \quad [11a]$$

$$\frac{d\epsilon_{i,j}}{dx} = \frac{1}{c_0}\frac{dc_{i,j}}{dx} = \frac{1}{c_0}\frac{c_j - c_i}{x_j - x_i} \quad [11b]$$

Equation 11b can be combined with Equation 8 to yield the following expression for materials during a first order phase transition between phases *i* and *j*.

$$\frac{\Delta G^f_{Li_{x_j}C_6} - \Delta G^f_{Li_{x_i}C_6}}{c_j - c_i} = \alpha_{i,j} \quad [12]$$

Where $\alpha_{i,j}$ is a constant for the phase transition *i* to *j*. Equation 9 can then be simplified in the following manner.

$$E_{cell} = \frac{d}{dx}\left[\alpha\, \epsilon_{Li_xC_6}\right] - \frac{d}{dy}\left[\beta\, \epsilon_{Li_yCoO_2}\right] \quad [13a]$$

$$\alpha = \begin{cases} -\frac{1}{F\epsilon_i}\, \Delta G^f_{Li_xC_6}, & x = x_i \\ -\frac{c_0}{F}\alpha_{i,j}, & x_i < x < x_j \end{cases} \quad [13b]$$

β in Equation 13a is defined analogously to α (Equation 13b) but for the LCO.

Applying Equation 13a to transition 1 (or any transition) in the graphite/LCO battery discussed above, Equation 13a simplifies to Equation 14.

$$E_{cell} \propto \frac{d}{dx}\left[\, \epsilon_{Li_xC_6}\right] - \frac{d}{dy}\left[\Delta G^f_{Li_yCoO_2}\right] \quad [14]$$

Using the fact that graphite is in a phase coexistence before transition 1 and a different phase coexistence after transition 1, both the voltage and dε/dx are step functions at transition 1. Another derivative produces Equation 15. Equation 15 changes the dependent variable from extent of lithiation, x, to state of charge, Q. dx/dQ is simply a constant factor and is absorbed by the proportionality constant. Here we also assume a

negligible or constant second derivative for the LCO free energy of formation in a single phase.

$$\frac{dE_{cell}}{dQ} \propto \frac{d^2\epsilon}{dQ^2} \quad [15]$$

During phase coexistence, such as during most of the graphite stages, both voltage and dε/dQ are a combination of pseudo-step functions with different magnitude steps, but steps that occur at the same locations. Thus, a simple model for battery electrodes yields that voltage is proportional to dε/dQ (Equation 14) and dV/dQ is proportional to $d^2\varepsilon/dQ^2$ (Equation 15). This supports the empirical relationship we proposed in **Figure 3c** and supported throughout this study. The reason why strain has larger, better defined peaks than voltage is likely due to the difference in lattice heights being more significant than the difference in free energy of formations. The small differences in free energy of formations results in the dV/dQ peaks becoming impossible to measure at higher charge rates (the step transition is a slow slope indistinguishable from the starting and ending plateaus) whereas the lattice height differences are large enough to produce a quantifiable peak even at faster rates. For example, transition 1 involves a step in equilibrium stage voltage from 120 mV to 85 mV in a graphite vs. Li system and a step in the lattice height from 0.353 nm to 0.37 nm, with an initial lattice height of 0.335 nm.[28,30] Transition 1 then has a 29% decrease in voltage and a 49% increase in strain, showing that strain has almost twice as much change as voltage at this transition.

3.7 Conclusions on the Strain-Voltage Relationship

In **Figure 7**, the results of the above derivation, primarily Equations 14 and 15, are shown schematically for two transitions (similar to the graphite system described above). The

expansion data is in red on top, with arrows indicating a derivative transformation between curves. The voltage data is in blue on the bottom, and the first derivative transformation is shown with an arrow. The proportionality between voltage and strain is highlighted by dashed lines at peaks in the dV/dQ and $d\varepsilon^2/dQ^2$ schematics.

The application of mechanical strain to characterize and model batteries has the potential to help researchers predict and understand material evolution during battery operation. Here, we show a fundamental relationship between $d^2\varepsilon/dQ^2$ and dV/dQ, namely that both strain and voltage contain information about electrode phase transitions and material evolution. Although in this work we use a model battery with graphite and LCO electrodes, electrode staging applies to other materials as well. This analysis can be generalized to other battery systems, but future work is necessary to verify this generalization, particularly with zero-strain materials. Because strain and voltage are intrinsically related and both are materials properties, the use of strain as a tool for characterizing battery materials has the potential to improve fundamental understanding of battery materials as well as aid in battery modeling and predictions. Additionally, our understanding of the coupling between mechanics and electrochemistry can be leveraged to improve energy harvesting applications by finding materials with larger coupling factors (see Equation 1) and optimizing the materials that already exist.

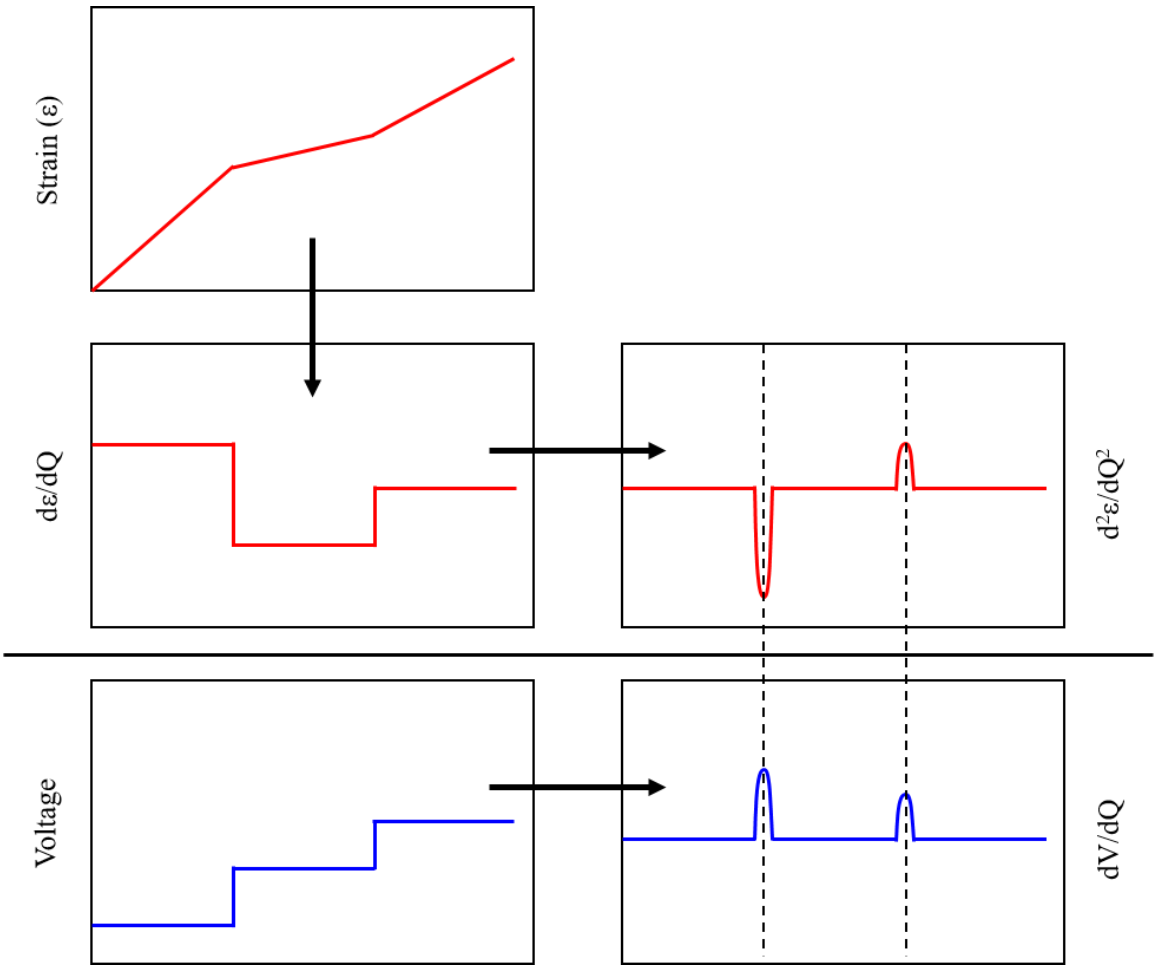

Figure 7. A schematic of derivatives to clarify the derivation of the relationship between $d^2\varepsilon/dQ^2$ and dV/dQ. The top three schematics are expansion (strain) derivatives (red) and the bottom two graphs are voltage derivatives (blue). Arrows indicate a derivative transformation between curves. The two transitions are schematically similar to a graphite system.

4 Fundamental Piezoelectrochemistry in Lithium Ion Batteries

4.1 Parameter Characterization

In general, there are many parameters that affect the energy harvesting system shown schematically in **Figure 1**. In this system, when one battery is compressed, the equilibrium potential changes and lithium ions (and electrons) move to equilibrate the potentials of the two batteries. However, both the equilibrium potential and the

mechanics of the system are strong functions of state of charge, as seen in **Section 3**. State of charge is therefore an extremely important parameter to investigate when considering energy harvesting. Other parameters of interest include: the stress applied (more stress correlates with more voltage) and the load resistance (voltage and power are functions of resistance). To maximize energy harvested, this work exclusively used the largest safe stress for batteries (15 MPa) and did not investigate other stress levels.

4.1.1 State of Charge

As shown in Equation 1, the coupling factor that determines the voltage increase at a given stress state is equal to the first derivative of strain with respect to state of charge (derived in detail in previous work).[3,8] In **Section 3.6**, we relate this derivative to electrode phase transitions, specifically the lattice heights and equilibrium potentials of the phases.

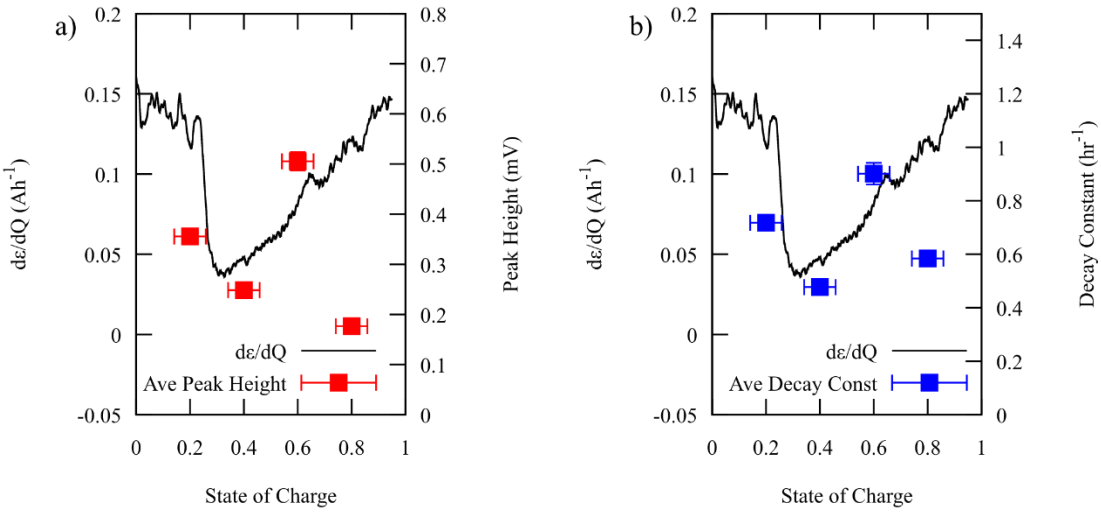

Figure 8. Comparison of the first derivative of strain (coupling factor) with parameters involved in energy harvesting, specifically average peak voltage height (a) and decay time constant (b). The ranges and scales on the second axes are chosen to best align the data for visual comparison to the strain derivative curve.

The same experiment from **Figure 2** is run at different states of charges, and the parameters of the voltage exponential decay are plotted and compared to dε/dQ in **Figure 8**. In **Figure 8a**, the average peak voltage is compared to the derivative of expansion. The axes ranges are picked to best visually compare the quantities. The measured heights and the derivative of expansion agree well and mostly have the same general trends, although there is significant error in some of the measurements. In **Figure 8b**, the average decay time constant is plotted for comparison to the derivative of expansion. Again, there is the same trend as dε/dQ. Notably, the points at 80% state of charge do not agree very well for either plot. This could be due to significantly increased resistance at this state of charge and stress or, especially in the case of the time constant, this could be due to the magnitude of dV/dQ at different states of charge. Overall, the data points match up remarkably well with dε/dQ, supporting the basic thermodynamic theory behind the coupling factor described in previous research, but more research is necessary to fully describe the system.[3,8] Because these parameters are proportional to dε/dQ, we can harvest the most energy by picking an optimal spot on the dε/dQ curve.

4.2 Different Harvesting Approaches with Lithium Ion Batteries

4.2.1 Self-Charging

In **Section 4.1**, we harvest energy using a load resistor, as seen in **Figure 1**. What happens, however, if the load disappears and instead the batteries are connected at both leads? Without a resistor, when the battery is compressed, the equilibrium potential of the electrodes will shift and lithium ions will move between electrodes (and electrons around the circuit) without dissipating work across the resistor. Over time, the state of

charge of the batteries will increase through repeated compression. This idea could be taken one step further by compressing only one half of the battery and letting the other half of the battery act as the reference/reservoir cell. This strategy of compressing one half of the battery and "self-charging" the battery is promising in theory but in practice is problematic. Primarily, the amount of energy that one would gain from compressing half the battery would be similar to the amounts described above, i.e., about 0.1 mJ. The 170 mAh batteries used in the above experiments store about 0.63 Wh of energy when fully charged, or 2268 J. This is seven orders of magnitude greater than the amount of energy we expect to add via "self-charging". When this theory is tested, the variation between different charge-discharge cycles is significantly greater than the amount of energy we assume is added per compression cycle (the variation was order 10^{-4} Wh or 1 J), so we cannot verify this theoretical self-charging mechanism. This method would be more effective in a different system where the coupling between voltage and stress is stronger.

4.2.2 Dynamic Energy Harvesting

In **Section 4.2.1**, the primary problem is that the amount of energy harvested is extremely small. While for some sensors, this amount of energy (order millijoules) may be sufficient, in general this amount of energy is too small for most applications and too small to measure relative to the amount of energy in a battery.[31] However, we hypothesize a different approach to energy harvesting that utilizes the mechanical-electrochemical coupling of lithium ion batteries but has the potential to generate orders of magnitude more energy. Looking closely at **Figure 1**, this apparatus uses compression at a fixed state of charge to generate a voltage and then lets this voltage decay, harvesting

energy as some small number of electrons traverses a load resistor. We know that the power generated is described with Ohm's law.

$$\mathrm{P} = \frac{(\Delta V)^2}{R} = I^2 R = I\Delta V \quad [16]$$

With the "static" energy harvester, we increase the voltage of a cell and let that voltage decay as power is dissipated over a resistor. But what if we apply a current to the battery in its compressed state to create a "dynamic" energy harvester? In general, when charging the battery, the power required is given by Equation 17.

$$\mathrm{P} = IV \quad [17]$$

When the battery is compressed, though, we increase the voltage by a small amount, ΔV. The power consumed during battery operation is now described by Equation 18.

$$\mathrm{P} = I(V + \Delta V) \quad [18]$$

Where ΔV is the same function of state of charge as described in Equation 1. In addition to increasing voltage, compression also increases internal resistance of commercial pouch cells. Specifically, compression closes pores in the polymer separator.[23] While we can ignore the separator for static energy harvesting, in this case the power consumed by the battery is now given by Equation 19, with the change in power relative to the uncompressed battery given by Equation 20.

$$\mathrm{P} = I(V + \Delta V) + I^2 \Delta R \quad [19]$$

$$\Delta\mathrm{P} = I(\Delta V + I\Delta R) \quad [20]$$

If $I < 0$, Equation 20 represents the additional amount of energy that can be retrieved from a compressed battery during discharge. To successfully harvest energy dynamically during discharge, in which the current is negative, we get the following inequality.

$$\Delta V > |I|\Delta R \quad [21]$$

In Equation 21, both the change in voltage and the change in resistance are functions of stress and state of charge. Optimally, we would increase the coupling factor from Equation 1 and decrease the resistance dependence of the separator (e.g., through a non-polymer separator). However, for commercial lithium ion batteries, the easiest way to produce energy through this method is to decrease the current. This reduces the effect of the resistance, but also decreases the overall power output.

In practice, to conduct this test, a 500 mAh battery (described in **Appendix A**) is used at 20% SOC. After allowing the voltage to relax, the battery is cycled by charging at 1 mA an additional 0.5 mAh and then discharging at 1 mA for 0.5 mAh repeatedly. This cycle produces consistent charge and discharge energy measurements. To test whether energy could be harvested as suspected in Equation 20, the battery is compressed to 10 MPa during discharge cycles and the "compressed" cycles are compared to the "uncompressed" cycles. Specifically, we compare the energy loss during each cycle:

$$\Delta E_i = E_{charge,i} - E_{discharge,i} \quad [22]$$

This metric was used to minimize environmental effects such as temperature since the entire cycle occurs within an hour period and should be in a consistent environment. In all cycles, we expect energy loss due to internal resistance. After initially running more than 20 compressed cycles to "prepare" the battery and remove any inelastic effects, the results of this experiment are shown in **Figure 9**

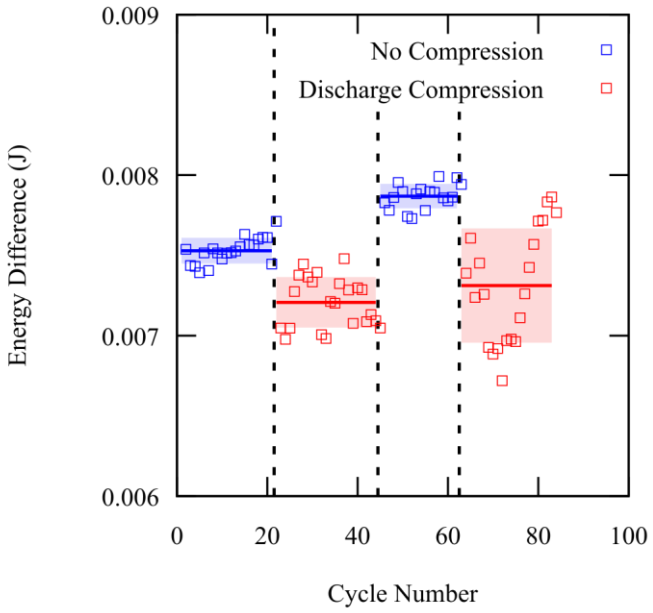

Figure 9. Dynamic energy harvesting during battery cycling. The blue data points are during uncompressed cycles and the red data points are during cycles in which the battery is compressed during discharge. The average of each set is indicated and the standard deviation of the points is shaded.

In **Figure 9**, the "compressed" cycle energy losses are shown in red and the "uncompressed" cycle energy losses are shown in blue. From the plot, the uncompressed cycles lost more energy than the compressed cycles. However, we can assume that the actual energy loss due to natural internal resistance and other loss mechanisms in the battery (excluding compression) is the same for all cycles. Thus, the difference in energy loss can be attributed to power being generated due to electrode compression, explaining why the compressed cycles "lost" less energy than the uncompressed cycles.

Comparing the compressed and uncompressed cycles, 0.43 ± 0.05 mJ is harvested per compressed cycle. Because each cycle has a period of 1 hour, this process produces, on average, 0.12 ± 0.01 μW of power. This is an order of magnitude better than the previously best reported piezoelectrochemical harvester using a graphite/LCO lithium ion battery system, which reported average power generation of 0.0136 μW.[8] A more optimal silicon system that harvested energy by applying torque (a slightly different form of piezoelectrochemistry) achieved 0.48 μW cm^{-2}.[9] Unfortunately, our method of energy

harvesting results in a power output independent of battery surface area, so a direct comparison is not possible, but the results are comparable at a glance since our batteries have an area of order 1 cm^2. The primary disadvantage to dynamic energy harvesting is that the energy is harvested during battery usage. Accordingly, energy cannot be harvested without expending energy, and the result is improved energy cycling efficiency, not net energy gain. However, **Figure 9** demonstrates that compression can improve the power output of a battery, and with a different battery (e.g., non-polymer separator), larger amounts of energy could be harvested. In any system, the amount of energy gained will still depend on the state of charge, and to optimize energy harvested, the pressure applied to the battery should be related to $d\varepsilon/dQ$ during discharge.

5 Applications of Piezoelectrochemistry to Other Systems

5.1 Solid-State Piezoelectrochemistry

In this work, we have discussed the applications of piezoelectrochemical properties of commercial lithium ion battery materials. However, these materials are not always ideal for harvesting energy using piezoelectrochemistry. As seen in Equation 1, the voltage to stress ratio is proportional to the derivative of strain with respect to state of charge. This quantity will be vastly different for different materials and will depend on the fundamental electrochemistry as well as lattice structures, according to Equation 13b. For example, in the graphite system used here, the maximum strain is about 3%, whereas for silicon systems, the maximum strain can be greater than 100%. A silicon electrode could potentially allow for significantly more energy to be harvested than the current commercial graphite electrodes.[8,9] In addition, systems that do not contain a polymer

separator would have the advantage of minimal resistance increase with pressure, allowing for increased dynamic energy harvesting, as described by Equation 20. Moving beyond lithium, a large variety of intercalation materials exist that, in theory, exhibit similar piezoelectrochemical properties characterized by Equation 15. With an ideal material, the efficiency and energy production of piezoelectrochemical harvesting can be greatly improved.

5.2 Capacitive Mixing and Osmosis

Above, we show how to use mechanical-electrochemical coupling in lithium ion batteries for energy harvesting applications. However, systems other than the traditional solid-state materials used in batteries also experience such coupling. Another system that exhibits electrochemical properties and is effected by external stresses is a basic osmosis device, as seen schematically in **Figure 10**. In this theoretical system, three chambers containing equal concentrations of NaCl (e.g. sea water) are separated by membranes that only allow water to pass (no ions). If a pressure is applied to chamber 2 (the middle chamber in **Figure 10a**), water will flow out into chamber 1and 3 through the membrane until the osmotic pressure balances with the hydrostatic pressure (**Figure 10b**). While this basic osmotic process may not seem very exciting, by applying a pressure we can create two solutions at different concentrations.

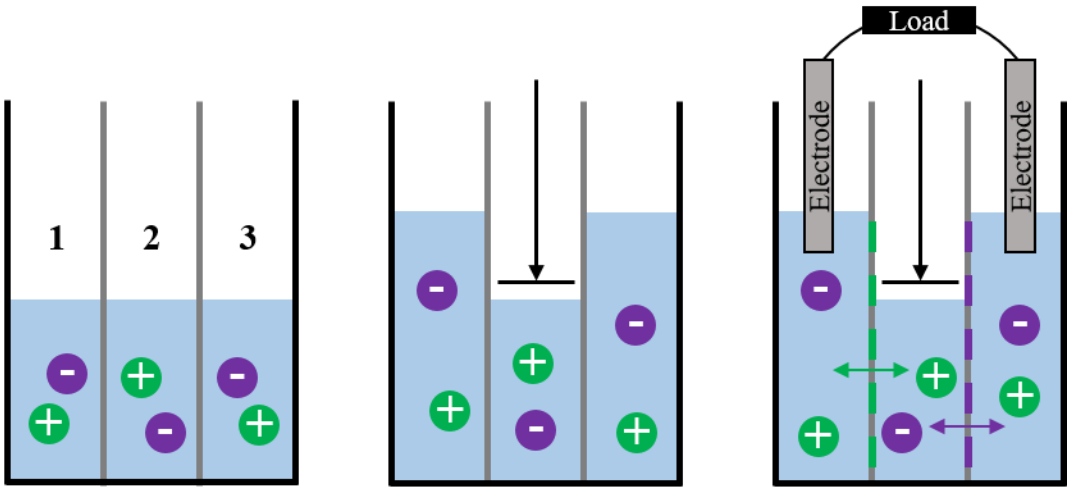

Figure 10. A basic salt solution with a water-permeable membrane (a), a salt solution with water-permeable membrane and an applied pressure (b), a salt solution in which the sodium ions can pass through one membrane and chlorine through the other (c).

Harvesting energy from salinity gradients by taking advantage of the entropy of mixing is a recent development, with theoretical efficiencies in flow processes of up to 95% and readily above 50%.[32,33] Some traditional strategies for harvesting energy that have been prototyped include pressure-retarded osmosis and reverse electrodialysis.[34–36] Very recently, capacitive mixing has been used to harvest this energy.[32,37] These techniques, in general, take flows of water with different salinities and harvest the energy available when they mix. The details of these methods are beyond the scope of this work, but the concept is interesting and important. Notably, all of these technique take two streams, one with higher salinity than the other, and harvest energy as the streams mix. However, no technique utilizes pressure to affect the salinity gradient. Some researchers have suggested using pressure to drive flow, but no research has been conducted on the use of pressure to increase the potential between solutions.[38] Ideally, added pressure will take advantage of osmosis to improve efficiency of capacitive mixing and flow battery technologies or to create an energy harvester.

As a simple extrapolation of the piezoelectrochemical effect to a completely different system, we consider the batch process described in **Figure 10c** and allow only Na^+ ions to pass through the membrane into chamber 1 and only allow Cl^- ions to pass through the membrane into chamber 3 (in addition to water passing through both membranes). The specific design parameters used in our setup are detailed in **Appendix D**. The model equations are modified slightly from capacitive mixing models described elsewhere.[32,39] In brief, this model describes ion transport in solution, current flow through the external load, ion transport through the membranes, and the creation of electrostatic double layers (EDLs) which form in the porous electrode.[40] We start by assuming ideal symmetry (i.e., the interactions between chambers 1 and 2 and between chamber 2 and 3 are identical except for the charge on the moving ion). We also assume ideal mixing, perfect blocking for the co-ion in the ion-specific membranes, and the Gouy-Chapman-Stern (GCS) model for a valid description of the EDLs in their equilibrium state (which happens quickly and is always be assumed to be valid).[41] Note that this theoretical model is a work in progress and is not meant to be quantitatively accurate or all-inclusive; it aims to demonstrate a proof of concept and the applicability of mechanical-electrochemical coupling to other systems. Due to symmetry, the equations are written in terms of chambers 1 and 2.

The first part of the model deals with the flow of water, essentially the basic osmotic pressure equation and conservation of mass.

$$\frac{\mathrm{dV_2}}{dt} = 2K_w A_{12}\left[P_{app} - \rho g(h_1 - h_2) - \left(c_{2,ions} - c_{1,ions}\right)RT\right] \quad [23]$$

$$V_1 = V_{1,initial} + (V_{2,initial} - V_2)/2 \quad [24]$$

In these equations, ρ is the density of water, g is the acceleration due to gravity, R is the ideal gas constant, T is the temperature (298 K in our case), K_w is the permeability of the membrane, and the factor of two comes from the symmetry.

The second part of the model deals with the change in ion number in chamber 2 (by electroneutrality, the ion number in chamber 1 remains constant because for every ion that crosses the membrane, one ion enters the EDL and "exits" the bulk). The equations describing the flow of sodium ions into chamber 2 are given by Equations 25 and 26.

$$\frac{\mathrm{dn_{Na,2}}}{dt} = -AJ/F \quad [25]$$

$$J = -KF\Delta\phi_{tr} \quad [26]$$

Where A is the membrane area, F is Faraday's constant, and J is the internal flux of sodium ions defined as a function of the potential drop across one half of chamber 2, chamber 1, and the membrane between. Equation 26 relates the ion flux to an overall potential that incorporates diffusion, membrane potentials, and overpotentials using an empirical transfer coefficient K described in **Appendix D**. All potentials here have been reduced by $V_T = RT/F$.

The cell voltage is given by Equation 27 and the external flux of charge by Equation 28, where the previously undefined potential terms refer to, in order, the Donnan potential, the potential of the EDL diffuse layer, and the potential of the EDL Stern layer (described in **Appendix D**).

$$\mathrm{V_{ext}} = 2V_T(\Delta\phi_{donnan} + \Delta\phi_d + \Delta\phi_{st} + \Delta\phi_{tr}) \quad [27]$$

$$\mathrm{V_{ext}} = AJR_{ext} \quad [28]$$

Here, R_{ext} is the external resistance or load. By using conservation of charge, namely that for every ion that crosses the membrane, one electron must travel around the circuit, the

above differential equations are solved in MATLAB (initial conditions described in **Appendix D**). First, using infinite resistance we measure the "open-circuit" voltage as a function of pressure, plotted in **Figure 11**.

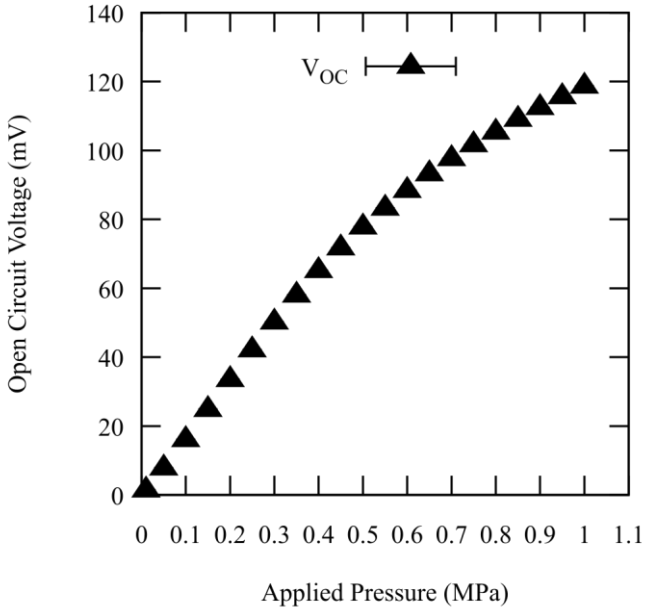

Figure 11. The V_{oc} of the system (calculated by letting the resistance approach infinity). Due to the nature of the simulations, the error bars on these data are smaller than the point size.

The open circuit voltage is effectively the Donnan potential across both membranes, and is greater than 100 mV at 1 MPa. Compared to the lithium ion batteries, which achieve voltages up to 0.5 mV at 15 MPa, this system appears significantly better. At pressures between 0.1 and 1 MPa, the apparent increase in voltage is one to three orders of magnitude larger than the voltage increases seen in commercial lithium ion batteries (and these simulated numbers are consistent with the order of magnitude of the literature values for capacitive mixing potentials).[3,32] Pressure was kept below 1 MPa for this system in order to keep water in chamber 2 and not "lose" it all to chamber 1.

The next part of the model uses a finite resistance (10 Ω in this case) and cycles the system using a pressure square wave to visualize whether energy harvesting occurs.

Figure 12a shows both the pressure applied and the voltage across the resistor as a function of time. **Figure 12b** shows the energy harvested and the energy input as functions of time (**Figure 12** is analogous to **Figure 2** for the lithium ion battery harvesting). In **Figure 12a**, the voltage has a similar form as found in **Figure 2** with the lithium ion battery harvesting. This simulation verifies that harvesting using a combination of osmotic pressure and salinity gradients should be feasible.

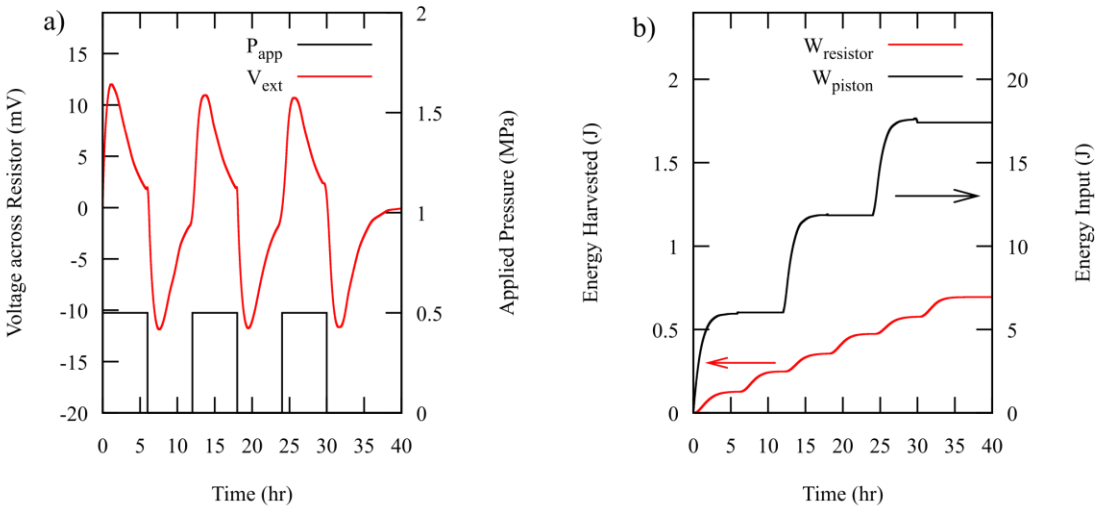

Figure 12. The voltage across the resistor and the applied pressure as functions of time (a), and the amount of energy harvested compared to the amount of energy input by the piston as functions of time (b).

This simulation shows that the peak voltage achieved for pressures of 0.5 MPa is 12 ± 1 mV, significantly less than the 78 mV predicted in **Figure 11** for the open circuit voltage at this pressure. This is likely due to transport restrictions in the system. These restrictions (diffusion through solution and across a membrane) slow down the current flow inside the cell, possibly causing the magnitude of the external resistance to play a more significant role in determining the peak voltage than it does with solid batteries.

The energy harvested and the energy input are given in **Figure 12b**. The average energy harvested per cycle is 0.23 ± 0.01 J and the average energy input per cycle is 5.9 ± 0.2 J. The average efficiency per cycle is 3.9 ± 0.2%. This is one to two orders of magnitude larger than efficiency reported above with lithium ion batteries, demonstrating the potential usefulness of this liquid system.

These simulations show that in an osmosis system, the coupling between pressure and voltage could be even more effective than in commercial lithium ion batteries for harvesting energy. However, these simulations use best-guess initial conditions and are useful only to determine trends, not quantitatively predict numbers. The above hypotheses that pressure can be used to harvest energy or improve efficiency need to be verified in experiment, but such experiments are beyond the scope of this work. All error is based on the change in output of the simulations given slightly different inputs.

6 Future Work

6.1 Piezoelectrochemistry and Energy Harvesting

The future work required in piezoelectrochemistry involves optimizing the systems described above. Most of the research up to this point on piezoelectrochemical materials has shown proof-of-concept devices that can harvest energy. However, with proper optimization of all parameters, such devices could become prevalent and more useful in applications ranging from wireless sensors to cell phone batteries. Additionally, the discovery and optimization of intercalation materials with more favorable coupling constants (Equation 1) would greatly improve the power output of piezoelectrochemical energy harvesting and are natural next steps in this research. Finally, the discussion in

Section 5.2 about the applications of pressure-voltage relationships for fluid systems such as flow batteries and capacitive mixing harvesters should be fully explored through more rigorous theory and experimentation.

6.2 Strain-Voltage Coupling

Future work on the relationship between strain and voltage is necessary to predict optimal harvesting strategies and to screen materials as harvesting candidates. Essentially, this future work would involve testing other materials and battery systems. Because of the theoretical analysis in **Section 3.6** we expect to find a relationship between the first derivative of voltage and the second derivative of strain in almost every intercalation system, but this must be verified with other battery materials such as silicon and germanium. Additionally, a longer aging study to build on **Section 3.5** is required to verify that the derivatives of strain behave in the same manner as the derivatives of voltage and can be used in aging analyses of batteries. While the work presented here primarily investigates the charging part of a battery cycle, observations during the experiments reveal some differences between the charging and discharging strain curves. The mechanical and electrochemical causes for these differences should be further investigated in the future. Last, the relationship between strain and voltage needs to be verified for dynamic charging schemes, i.e., partial charging of the battery, which is more realistic of practical battery usage. These future work paths would improve our understanding of strain-voltage coupling and enable us to predict battery aging, design better battery materials, and improve safety monitoring of battery cells. This future work

would also give us the opportunity to find materials with the desired characteristics for energy harvesting, namely large coupling factors.

7 Conclusions

In this work, we investigate energy harvesting using lithium ion batteries and the fundamental relationship between mechanics and electrochemistry that makes such harvesting possible. Specifically, this work initially explores the piezoelectrochemical effect in commercial lithium ion batteries. However, a complete understanding of piezoelectrochemical energy harvesting requires knowledge of mechanical-electrochemical coupling. We therefore explore how changes in battery state of charge affect the voltage and the electrode mechanics, developing a theoretical justification for voltage-strain coupling and proposing that strain could be a more useful tool for characterizing electrodes at higher charge rates in energy storage applications.

We then explore piezoelectrochemistry in depth. Using knowledge of the mechanical-electrochemical coupling, we begin to characterize energy harvesting devices that use battery materials. We also propose new methods for harvesting energy from lithium ion batteries such as dynamic harvesting. We finish our discussion of piezoelectrochemical applications by proposing that a similar coupling could exist in a liquid system with dissolved ions and that this system (a capacitive mixing harvester or flow battery) could have a much larger coupling factor than that of lithium ion battery materials.

8 Works Cited

(1) Ramadesigan, V.; Northrop, P. W. C.; De, S.; Santhanagopalan, S.; Braatz, R. D.; Subramanian, V. R. *J. Electrochem. Soc.* **2012**, *159* (3), R31.
(2) Scrosati, B.; Garche, J. *J. Power Sources* **2010**, *195* (9), 2419.
(3) Cannarella, J.; Leng, C. Z.; Arnold, C. B. **2014**, *9115*, 91150K.
(4) Xu, S.; Hansen, B. J.; Wang, Z. L. *Nat. Commun.* **2010**, *1* (7), 93.
(5) Wang, Z. L.; Song, J. *Science* **2006**, *312* (5771), 242.
(6) Qin, Y.; Wang, X.; Wang, Z. L. *Nature* **2008**, *451* (7180), 809.
(7) Koka, A.; Sodano, H. a. *Adv. Energy Mater.* **2014**, n/a.
(8) Cannarella, J.; Arnold, C. B. *Adv. Mater.* **2015**, n/a.
(9) Kim, S.; Choi, S. J.; Zhao, K.; Yang, H.; Gobbi, G.; Zhang, S.; Li, J. *Nat. Commun.* **2016**, *7*, 10146.
(10) Schiffer, Z. J.; Cannarella, J.; Arnold, C. B. *J. Electrochem. Soc.* **2016**, *163* (3), A427.
(11) Goodenough, J. B.; Kim, Y. *Chem. Mater.* **2010**, *22* (3), 587.
(12) Smith, a. J.; Dahn, H. M.; Burns, J. C.; Dahn, J. R. *J. Electrochem. Soc.* **2012**, *159* (6), A705.
(13) Bloom, I.; Jansen, A. N.; Abraham, D. P.; Knuth, J.; Jones, S. a.; Battaglia, V. S.; Henriksen, G. L. *J. Power Sources* **2005**, *139* (1-2), 295.
(14) Deshpande, R.; Verbrugge, M.; Cheng, Y.-T.; Wang, J.; Liu, P. *J. Electrochem. Soc.* **2012**, *159* (10), A1730.
(15) Cannarella, J.; Arnold, C. B. *J. Power Sources* **2014**, *269*, 7.
(16) Dahn, H. M.; Smith, a. J.; Burns, J. C.; Stevens, D. a.; Dahn, J. R. *J. Electrochem. Soc.* **2012**, *159* (9), A1405.
(17) Oh, K. Y.; Siegel, J. B.; Secondo, L.; Kim, S. U.; Samad, N. a.; Qin, J.; Anderson, D.; Garikipati, K.; Knobloch, A.; Epureanu, B. I.; Monroe, C. W.; Stefanopoulou, A. *J. Power Sources* **2014**, *267*, 197.
(18) Bitzer, B.; Gruhle, A. *J. Power Sources* **2014**, *262*, 297.
(19) Fu, R.; Xiao, M.; Choe, S. Y. *J. Power Sources* **2013**, *224*, 211.
(20) Mohan, S.; Kim, Y.; Siegel, J. B.; Samad, N. a.; Stefanopoulou, a. G. *J. Electrochem. Soc.* **2014**, *161* (14), A2222.
(21) Sethuraman, V. A.; Winkle, N. Van; Abraham, D. P.; Bower, A. F.; Guduru, P. R. *J. Power Sources* **2012**, *206*, 334.
(22) Sommer, L. W.; Raghavan, A.; Kiesel, P.; Saha, B.; Schwartz, J.; Lochbaum, A.; Ganguli, A.; Bae, C.-J.; Alamgir, M. *J. Electrochem. Soc.* **2015**, *162* (14), A2664.
(23) Cannarella, J.; Arnold, C. B. *J. Power Sources* **2013**, *226*, 149.
(24) Hahn, M.; Buqa, H.; Ruch, P. W.; Goers, D.; Spahr, M. E.; Ufheil, J.; Novák, P.; Kötz, R. *Electrochem. Solid-State Lett.* **2008**, *11* (9), A151.
(25) Barker, J. *Electrochim. Acta* **1999**, *45* (1), 235.
(26) Reimers, J. N.; Dahn, J. R. **1992**, *139* (8), 2.
(27) Dahn, J. R. *Phys. Rev. B* **1991**, *44* (17).
(28) Ohzuku, T. *J. Electrochem. Soc.* **1993**, *140* (9), 2490.
(29) Vetter, K. J. *J. Electrochem. Soc.* **1963**, *110* (6), 597.
(30) Takami, N. *J. Electrochem. Soc.* **1995**, *142* (2), 371.
(31) Shnayder, V.; Hempstead, M.; Chen, B.-R.; Allen, G. W.; Welsh, M. *Proc. 2nd*

Int. Conf. Embed. networked Sens. Syst. SenSys 04 **2004**, 188.
(32) Sales, B. B.; Saakes, M.; Post, J. W.; Buisman, C. J. N.; Biesheuvel, P. M.; Hamelers, H. V. M. *Environ. Sci. Technol.* **2010**, *44* (14), 5661.
(33) Vermaas, D. A.; Veerman, J.; Yip, N. Y.; Elimelech, M.; Saakes, M.; Nijmeijer, K. *ACS Sustain. Chem. Eng.* **2013**, *1* (10), 1295.
(34) Post, J. W.; Hamelers, H. V. M.; Buisman, C. J. N. *Environ. Sci. Technol.* **2008**, *42* (15), 5785.
(35) Gerstandt, K.; Peinemann, K.-V.; Skilhagen, S. E.; Thorsen, T.; Holt, T. *Desalination* **2008**, *224* (1–3), 64.
(36) WEINSTEIN, J. N.; LEITZ, F. B. *Science (80-.).* **1976**, *191* (4227), 557.
(37) Brogioli, D.; Ziano, R.; Rica, R. a.; Salerno, D.; Kozynchenko, O.; Hamelers, H. V. M.; Mantegazza, F. *Energy Environ. Sci.* **2012**, *5*, 9870.
(38) Lu, M.-C.; Satyanarayana, S.; Karnik, R.; Majumdar, A.; Wang, C.-C. *J. Micromechanics Microengineering* **2006**, *16* (4), 667.
(39) Brogioli, D.; Ziano, R.; Rica, R. A.; Salerno, D.; Mantegazza, F. *J. Colloid Interface Sci.* **2013**, *407*, 457.
(40) Bazant, M. Z.; Thornton, K.; Ajdari, A. *Phys. Rev. E* **2004**, *70* (2), 21506.
(41) Biesheuvel, P. M. *J. Colloid Interface Sci.* **2004**, *275* (2), 514.
(42) Marks, T.; Trussler, S.; Smith, A. J.; Xiong, D.; Dahn, J. R. *J. Electrochem. Soc.* **2011**, *158* (1), A51.
(43) Zhang, S.; Ding, M. S.; Xu, K.; Allen, J.; Jow, T. R. *Electrochem. Solid-State Lett.* **2001**, *4* (12), A206.
(44) Zhao, R.; Biesheuvel, P. M.; Miedema, H.; Bruning, H.; van der Wal, A. *J. Phys. Chem. Lett.* **2010**, *1* (1), 205.

9 Funding Acknowledgements

Funding for materials used during summer portions of this work (parts of **Section 3** and **Appendices A**, **B**, and **C**) provided by the Michelle Goudie ’93 Summer Fellowship in Environmental Studies. Funding for materials for the rest of this work provided by SEAS Lidow Independent Work/Senior Thesis fund.

10 Appendix

A Experimental Methods for Measuring Battery Strain

This section is taken and modified from the author’s publication on this work and represents work done during the 2015 summer.[10]

This research used commercial pouch cells with 500 mAh nominal capacity (used for calculating C-rates) and nominal dimensions of 25 mm by 35 mm by 6.5 mm. The active materials in the cells are lithium cobalt oxide and graphite, and $LiPF_6$ is the electrolyte in organic solvent. One charge/discharge cycle of a battery consists of a constant current charge step to 4.2 V, a constant voltage charge step until the current decays below a twentieth of the maximum capacity, a rest step for one hour, a constant current discharge step to 2.7 V, then a final rest step of at least an hour. For the high-rate test, I used a commercial pouch cell designed to be charged at 1C with 2000 mAh nominal capacity and nominal dimensions of 50 mm by 60 mm by 5.8 mm. The active materials in these cells are lithium cobalt oxide and graphite, and $LiPF_6$ is the electrolyte in organic solvent.

The dilatometer setup described in **Figure A1** is used to perform all mechanical measurements in this study. The LVDT sensor moves 50 microns per 1 V measured, and the accuracy of the dilatometer is 0.2 microns. The entire setup is inside an oven at 35 °C to avoid temperature effects on both the battery and the setup. All results from the dilatometer is read using an Arbin MITS Pro software with a potentiostat.

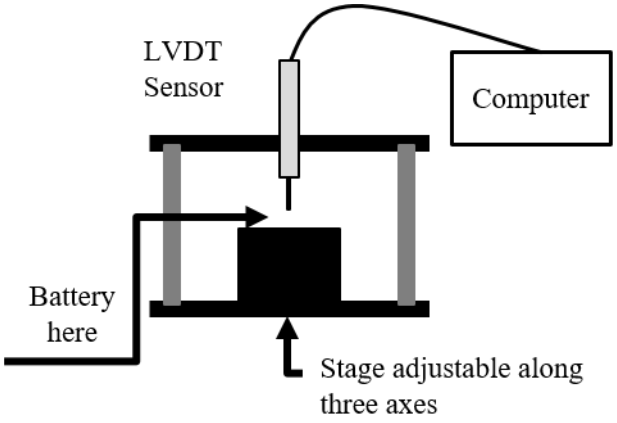

Figure A1. A schematic of the dilatometer used in this experiment. The battery is placed under an LVDT sensor to measure expansion and the entire setup is kept at 35 °C.

Analysis of the data is done with MATLAB. All derivatives are simply the quotient $\frac{\Delta y}{\Delta x}$, and any functional fits were performed using the MATLAB fit function. I recorded data every 0.5 seconds from the LVDT and every 1 s from the battery. All results are filtered using MATLAB's implementation of a Savitzky-Golay filter, a filter that essentially replaces every *n* data points with a least-squares line where *n* increases as the C-rate decreases to account for more data points per cycle.

Part of our analysis required converting from state of charge, or fraction maximum capacity, to *x* in Li_xC_6 in order to compare against literature values. This conversion is a constant factor, specifically the fraction of the graphite capacity utilized in the battery compared to the maximum capacity available in the graphite. To calculate

this fraction, I made coin cells of Li vs graphite and LCO vs graphite using 7/16" diameter LCO and graphite electrodes harvested from the commercial batteries described above.[42] The capacity of the LCO vs graphite coin cells was divided by the capacity of the Li vs graphite coin cells (representing the full lithiation of the graphite electrode) to produce a factor for converting from state of charge to extent of graphite lithiation in these particular batteries. This conversion relies on the assumption that x = 0 at SOC = 0 (2.7V in our case). The calculation of this factor is given with the analysis.

B Quantitative Comparison of dV/dQ and $d^2\varepsilon/dQ^2$

This section is taken and modified from the author's publication on this work and represents work done during the 2015 summer.[10]

In this section, a quantitative comparison of the peaks seen in **Figure 1** (reproduced here as **Figure B1**) is given and discussed.

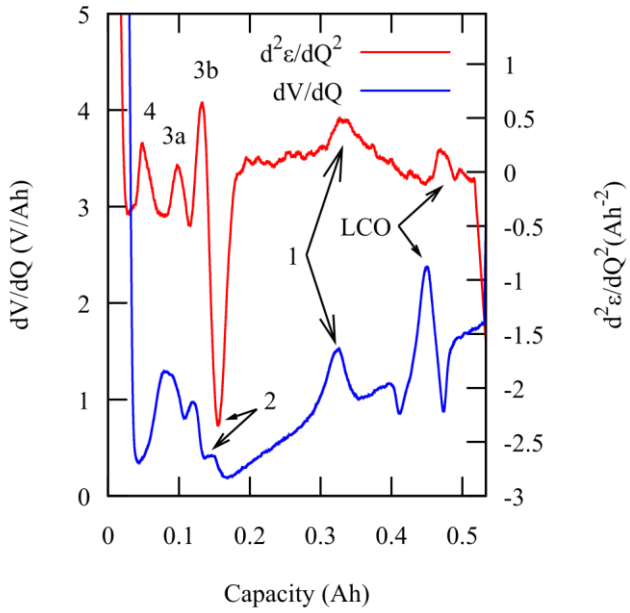

Figure B1. Reproduction of **Figure 1c**. $d^2\varepsilon/dQ^2$ and dV/dQ for a commercial battery cycling at C/20. Select transitions are labeled and the similarity between the $d^2\varepsilon/dQ^2$ and dV/dQ peaks is visually apparent.

A simple method of quantification is to record the state of charge at which the maximum of a transition peak occurs. Another method for quantifying transition peaks is through a standard Gaussian fit. Gaussian fits have the added advantage of providing a peak width and height, a more difficult value to measure by eye due to noise in the data. The center of the Gaussian fit has the same location as the maximum value in a transition peak, so these methods are interchangeable when only looking at the exact point a transition occurs. The peak positions, using either a maximum or the center of a Gaussian fit, are given in **Table B1** along with literature values for graphite transitions.[30] The transition numbering corresponds to the graphite stage following the transitions according to Reference [17] and select transitions are indicated in **Figure B1**. All values in **Table B1** are for *x* in Li_xC_6 for best comparison to literature and generality. Conversion from state of charge (the units of **Figure B1**) to *x* is done by multiplying the capacity by the maximum fraction of graphite lithiated in the batteries, using x = 0 at SOC = 0 (2.7 V). This fraction was determined by making coin cells of graphite vs Li and graphite vs LCO using electrodes from a commercial battery and comparing the capacities (2.90 ± 0.09 mAh and 2.60 ± 0.08 mAh, respectively). The conversion factor is then 0.90 ± 0.04, a reasonable value that makes sense because batteries often have some excess capacity.

Table B1. Comparison of graphite transition peaks in expansion data, voltage data, and literature[30]

Transition	x from Expansion*	x from Voltage*	Graphite x
4	0.07 ± 0.01	--	0.04
3a	0.17 ± 0.01	0.13 ± 0.01	0.12
3b	0.22 ± 0.01	0.20 ± 0.01	0.21
2	0.26 ± 0.02	0.24 ± 0.01	0.27
1	0.56 ± 0.03	0.54 ± 0.03	0.5
LCO	0.79 ± 0.04	0.76 ± 0.03	--

* All error is 1σ

In **Table B1**, the peaks in the expansion, voltage, and literature transitions align, supporting our proposed relationship between $d^2\varepsilon/dQ^2$ and dV/dQ. Small discrepancies between literature values and our experimental results are expected, especially in the region below $x = 0.3$, where the transitions are much less clearly defined. In this region, there are dilute graphite phases and a potential LCO phase transition, and identifying exact phases in the graphite and LCO is beyond the scope of this paper. In **Figure B1**, the peak representing transition 2 in the voltage data is more a plateau than a peak. To quantify this transition in **Table B1**, we used the center of the plateau (which was a very slight peak). In the data above, transition 4 (occurring at the lowest state of charge) is not present in the voltage data but is clear in the expansion data. This transition is a known graphite transition, and the fact that it appears in the strain data but not in the voltage is a benefit to characterizing electrodes with strain and could add to previous studies of SEI formation on graphite at low voltages.[43] One trend in the comparison of dV/dQ and

$d^2\varepsilon/dQ^2$ is that the strain peaks consistently occur at slightly higher states of charge than the voltage peaks during battery charging.

C Strain and Voltage Peaks at Various Charge Rates

This section is taken and modified from the author's publication on this work and represents work done during the 2015 summer.[10]

While **Figure 2** visualizes how charge rate affects voltage and strain, in **Figure C1**, parameters from a Gaussian fit for transition 1 in the $d^2\varepsilon/dQ^2$ are compared to the Gaussian parameters for this transition in the dV/dQ plot. In **Figure C1a**, the heights of the Gaussian fits are displayed for strain and voltage. At rates larger than 0.3C, the peak in dV/dQ is indistinguishable from the noise and cannot be measured. However, although there is not a recognizable transition in the voltage data, there is a consistent Gaussian transition in the strain data. In **Figure C1b**, the position of the transition is displayed in the voltage and the strain data. At slower charging rates, the transition occurs at higher states of charge in both voltage and strain. Additionally, the strain transition consistently occurs at higher states of charge than the voltage transition and is much less dependent on charge rate than voltage. The transition peak shifts more than 15% between 0.05C and 0.3C in the dV/dQ data but shifts less than 10% between 0.05C and 0.5C in the strain data. Overpotentials in this system could explain why the voltage transition appears at lower states of charge than the strain transition during charging because the overpotential should minimally impact the strain but can significantly affect the voltage. Although **Figures 2** and **C1** represent data from only one battery cell, these

trends and similar results were found in multiple cells. Overall, we conclusively show with **Figures 2** and **C1** that strain is a more practical tool than voltage for identifying stage transitions at higher rates.

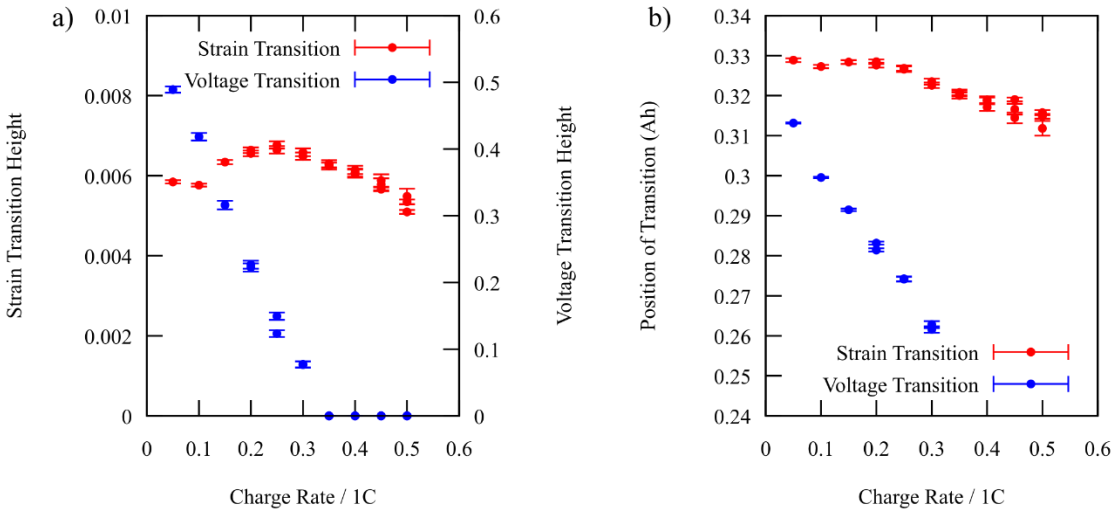

Figure C1. Gaussian parameters for transition 1. The height of transition (a) and the position of the transition (b). The heights of the transition are in arbitrary units. Error bars represent 95% confidence on fit parameters. Note that the strain transition remains visible up to C/2 whereas the voltage transition does not. The voltage transition also shifts with charge rate significantly more than the strain transition.

D Details of Capacitive Mixing Simulation

In this section, some of the technical details of the simulations performed in **Section 5.2** are given. This model is modified from previous work and is a work in progress.[32,44] It is meant to be qualitatively accurate and to show trends. Please refer to **Figure 10** for a qualitative rendering of the system. Chamber 2 has an area of 30 cm^2 and a height of 5 cm. Chamber 1 (3) has an area of 5 cm^2 and a height of 5 cm. The exchange area between chambers is 20 cm^2 (the depiction in **Figure 10** would have to be modified to allow for this exchange area at the various water heights that occur during the process).

The initial concentration of the system is 68 mM. The equations used to model the water flow in this system are (reproduced from above):

$$\frac{\mathrm{dV}_2}{dt} = 2K_w A_{12}\left[P_{app} - \rho g(h_1 - h_2) - \left(c_{2,ions} - c_{1,ions}\right)RT\right] \quad \text{[D1]}$$

$$V_1 = V_{1,initial} + (V_{2,initial} - V_2)/2 \quad \text{[D2]}$$

In these equations, ρ is the density of water, g is the acceleration due to gravity, R is the ideal gas constant, T is the temperature (298 K in our case), K_w is the permeability of the membrane (order of magnitude 10^{-11} m^3/m^2-s-Pa), and the factor of two comes from the symmetry.

The second part of the model deals with the change in ion number in chamber 2 (by electroneutrality, the ion number in chamber 1 remains constant because for every ion that crosses the membrane, one ion enters the EDL and "exits" the bulk). The equation describing the flow of sodium ions into chamber 2 is given by a combination of Fick's laws and electrostatics.

$$\frac{\mathrm{dn}_{\mathrm{Na},2}}{dt} = -AJ/F \quad \text{[D3]}$$

$$J = -KF\Delta\phi_{tr} \quad \text{[D4]}$$

Where A is the membrane area, F is Faraday's constant, and J is the internal flux of sodium ions defined as a function of the potential drop across one half of chamber 2, chamber 1 and the membrane between. Equation D4 relates the ion flux to an overall potential that incorporates diffusion, membrane potentials, and overpotentials using an empirical transfer coefficient K. All potentials here have been reduced by $V_T = RT/F$. The transfer coefficient is given by the following:[44]

$$K^{-1} = K_m^{-1} + \left(0.5c_{Na,2} + 10\right)^{-1} + \left(0.5c_{Na,1} + 10\right)^{-1} \quad \text{[D5]}$$

Where $K_m = 35\ \mu mol/(m^2 s)$ and K has the same units.

The cell voltage is given by Equation D6 and the external flux of charge by Equation D7, where the potential terms not described previously refer to, in order, the Donnan potential, the potential of the EDL diffuse layer, and the potential of the EDL Stern layer.

$$\mathrm{V_{ext}} = 2V_T(\Delta\phi_{donnan} + \Delta\phi_d + \Delta\phi_{st} + \Delta\phi_{tr}) \quad [D6]$$

$$\mathrm{V_{ext}} = AJR_{ext} \quad [D7]$$

$$\Delta\phi_{\mathrm{donnan}} = \ln(c_{Na,2}/c_{Na,1}) \quad [D8]$$

$$\Delta\phi_{\mathrm{d}} = 2\sinh^{-1}\left(\frac{qF}{A_{elec}}\frac{1}{4r_{debye}c_{Na,1}F}\right) \quad [D9]$$

$$\Delta\phi_{st} = -\frac{qF}{A_{elec}}\frac{1}{C_{st}V_T} \quad [D10]$$

$$\mathrm{r_{debye}} = \left(8\pi c_{Na,1}N_a\lambda_B\right)^{-1/2} \quad [D11]$$

Note that here q is the number of moles of charge on the electrodes (decreasing as the number of ions in chamber 2 increases), A_{elec} is the electrode area (assumed to be 2000 m^2 for a porous electrode), C_{st} is the Stern layer capacity (0.1 F/m^2), N_a is Avogadro's number, and λ_B is the Bjerrum length (0.72 nm in water at room temperature).